ASEAN Engineering Journal

Full Paper

A GEOMETRIC DESIGN METHOD OF RADIAL INFLOW TURBINE FROM 0D TO 3D FOR ORGANIC RANKINE CYCLE MICRO POWER GENERATION

Ari Darmawan Pasek[a], Prihadi Prasetyo[a], Asybel Bonar[a], Maulana Arifin[b]

[a]Faculty of Mechanical and Aerospace Engineering, Institut Teknologi Bandung, Jl. Ganesha no.10, Bandung (40132), Indonesia
[b]Research Centre for Electrical Power and Mechatronics, Indonesian Institute of Sciences – LIPI, Indonesia

Article history
Received
28 June 2021
Received in revised form
01 September 2021
Accepted
09 September 2021
Published online
28 February 2022

*Corresponding author
aripasek@itb.ac.id

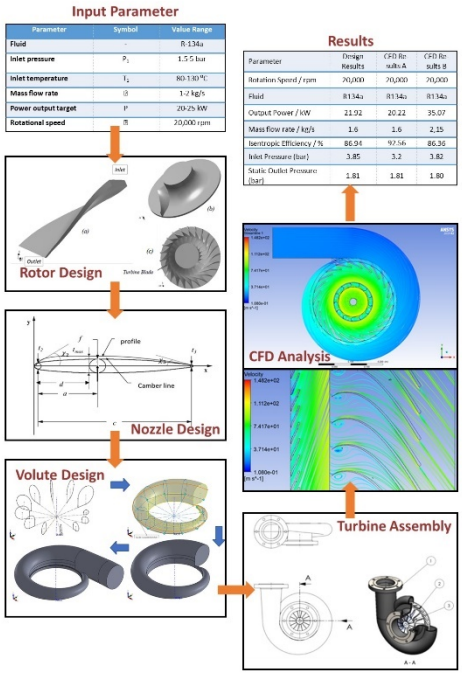

Abstract

Radial turbine is an essential component of Organic Rankine Cycle system and requires a medium to high specific speed turbine. Radial turbine has a compact structure that can easily be made with current additive manufacturing technology if the 3D geometry of turbine components is known. Current researches only conduct 2D geometry design then import it into third-party software to construct the 3D geometry. This paper will explain design methodology to design radial inflow turbines from 0D until 3D using simple tools. The methods used to determine the geometry were based on Aungier, with modification in determining value of a, b, and c in nozzle design and A1 in Volute design to simplify the design process. The tools used in design were MS Excel and Autodesk Inventor. Rotor design starts with determining the two-dimensional parameters. All parameters are calculated based on the angle and velocities occurring in the velocity triangle at the inlet and outlet of the rotor using equations proposed by Aungier. Then, the straight, radial and quasi-normal lines of the blades are drawn based on governing equations. The transformation from 2D to 3D blade coordinates is done by using vector equations. The nozzle is designed by drawing the camber line profile and calculating the nozzle thickness to get the profile based on the governing equations given by Aungier. The volute dimensions are obtained by calculating the area of volute inlet passage and mean radius from mass and momentum conservation equations. A case study is shown in this paper with R134a as working fluid with the following range inlet conditions: mass flow rate at 1-2 kg/s, inlet pressure at 1.5 to 5 bar, inlet temperature at 80 to 130 °C, and power output target between 20 to 25 kW. The CFD results show that the designed turbine performs well with slight wake flow at the pressure side on the rotor inlet. A further study needs to be done in order to check the validity of this method by conducting analysis through experimental.

Keywords: Radial Inflow Turbine, Organic Rankine Cycle, Power Generations, Design Method, CFD Simulation

1.0 INTRODUCTION

New and renewable energy contribute significantly to the national energy supply in developed countries [1] as well as in developing countries[2]. The Organic Rankine Cycle (ORC) system is suitable for utilizing low temperature heat [3] for power generation, such as heat from geofluid, waste heat, solar heat and biomass combustion [4]. The system uses organic fluids such as halocarbons and hydrocarbons as working fluid [5]. ORC can supply additional power even with low thermal efficiency [6].

System efficiency also depends on turbine geometry [7]. Hence, it is important to develop a design method to determine the ORC turbine geometry. Several authors have studied methods to design micro radial turbines. The overview of some turbines builds for ORC shown in Table 1.

Table 1 Review of works in radial turbine design for ORC for micro power generation application [6,8–11]

Author	Output (kW)	Efficiency (%)	Working Fluid
Alshammari et al.	20-25	30-35.2	R-134a
Fiaschi, et al.	5	69	R-134a
Kang, S.H.	190	84	R-245fa
Jubori, A.M, et al.	13.6	79.05	n-Pentane
Costall, A.W, et al.	45.6	56.1	Toluene
Costall, A.W, et al	24	79	R-245fa

The design method was first introduced in [12]. The equations used in the design were developed by Aungier [13]. A general method for designing radial turbines has been introduced in [14], while a preliminary design has been proposed in [15]. However, both papers only discuss the design of 2D parameters. Two other papers [15,16] reported a numerical simulation to show the influence of important geometric parameters on turbine performance and in [17] a thermodynamic consideration on the radial inflow turbine design is discussed.

This paper will clearly describe the method to design rotor, nozzle, and volute geometry for radial inflow turbines. The equations were introduced by Aungier, arranged in a more systematic order with some modification. The modifications were when designing preliminary parameters, where the results were evaluated at 5 conditions chosen from several resources. Calculation values of a, b, and c when designing nozzle and A1 when designing Volute were taken iteratively. Also, the coordinate of meridional lines was determined with the help of 3D Drawing software to simplify the process. The design process of radial turbine was shown in figure 1.

2.0 BLADE ROTOR GEOMETRY

The blade rotor of an inflow radial turbine is schematically shown in Figure 2, divided into several radial and axial sections. Station 1 indicates the inlet volute station, station 2 indicates the inlet to the nozzle, station 3 indicates the outlet of the nozzle, stations 4 and 5 indicate the inlet and outlet of the blades, and station 6 indicates the outlet of the exhaust diffuser. The design started by selecting its operating condition: total temperature at inlet volute, T_{t1}; the inlet total pressure P_{t1}; the fluid mass flow rate, $\dot{m}$; and the pressure ratio, $\frac{P_{t1}}{P_{t5}}$, followed by selecting a working fluid. Then, rotational speed n_s can be calculated with:

$$n_s = \frac{\omega\sqrt{Q_5}}{(\Delta H_{id})^{0.75}} \quad (1)$$

where w is the angular velocity in rad/s, which can be derived from rotational speed n_s. Q_5 is the volumetric rate in m^3/s, which can be calculated from the mass flow rate $\dot{m}$, with density is taken at station 5(ρ_5). ΔH_{id} is the isentropic enthalpy difference of the working fluid. Then, *vs* can be calculated from [17]

$$v_s = \frac{U_4}{C_{0s}} = 0.737{n_s}^{0.2} \quad (2)$$

The jet velocity C_{0s} and the tangential velocity at rotor inlet, U_4, can be calculated from [17] as shown in equation (3)

$$C_{0s} = \sqrt{2\Delta H_{id}}\, U_4 = v_s C_{0s}\,\} \quad (3)$$

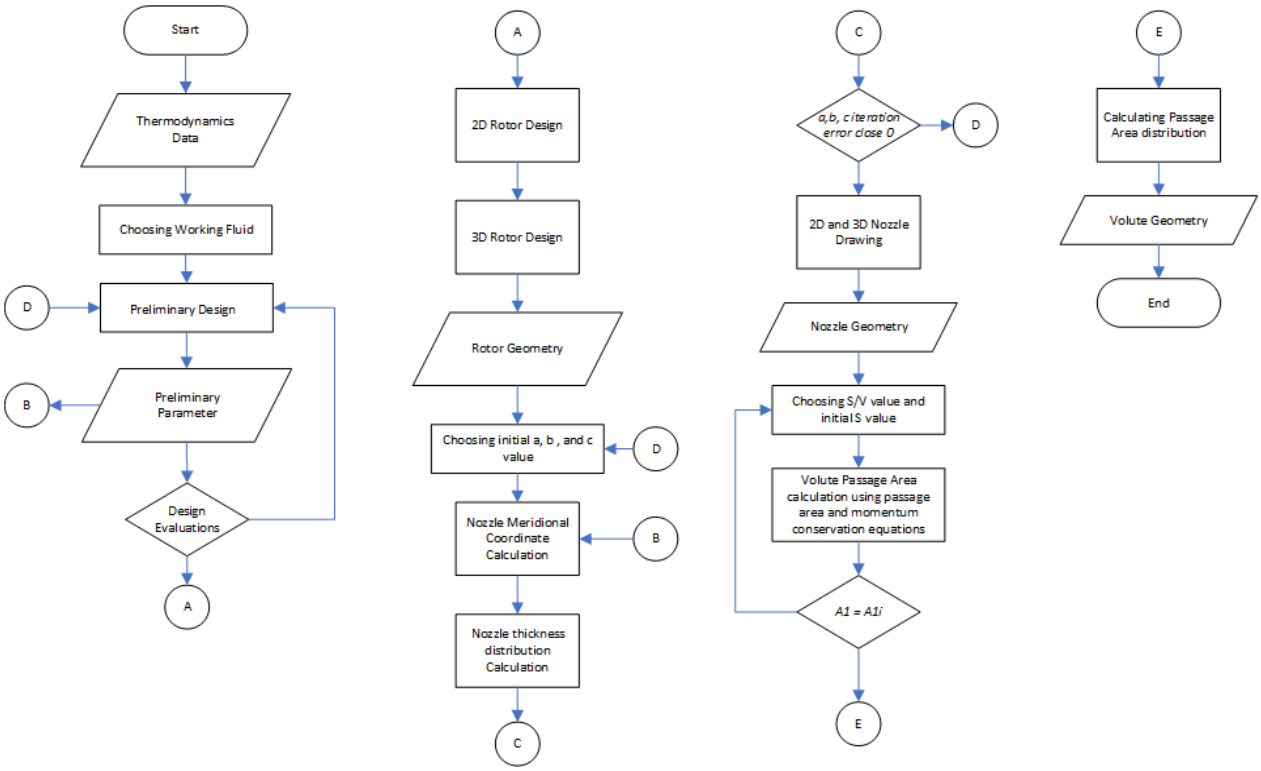

Figure 1 Radial Turbine Design Process

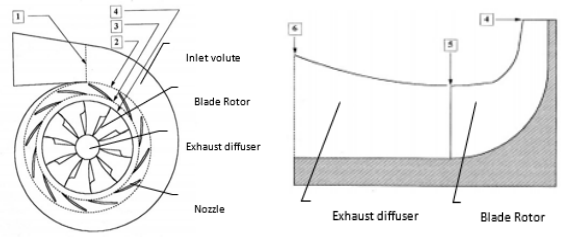

Figure 2 Radial inflow turbine with its sections

The total-static efficiency was calculated by

$$\eta_s = 0.87 - 1.07(n_s - 0.55)^2 - 0.5(n_s - 0.55)^3 \quad (4)$$

Figure 2 shows the U_4 and other velocities in the inlet and outlet of the blade rotor, and Figure 3 (b) shows some rotor dimensions that must be determined. Referring to these figures, the inlet rotor radius r_4 is calculated from

$$r_4 = \frac{U_4}{\omega} \quad (5)$$

Meanwhile, the inlet rotor passage is determined by using the following equations [17]:

$$b_4 = \frac{\dot{m}}{2\pi r_4 \rho_4 C_{m4}} \quad (6)$$

$$C_{m4} = C_{\theta 4} \, tan \, tan \, \alpha_4 \quad (7)$$

$$C_{\theta 4} = \frac{U_4 \eta_s}{2{v_s}^2} \quad (8)$$

$$\alpha_4 = 10.8 + 14.2{n_s}^2 \quad (9)$$

The density at the rotor inlet, ρ_4, is determined by iteratively using the following equation [17]:

$$h_4 = H_4 - \frac{1}{2}\left({C_{m4}}^2 + {C_{\theta 4}}^2\right) P_4 = P_{t4} - \frac{1}{2}\rho_4 {C_4}^2 C_4 = \sqrt{{C_{m4}}^2 + {C_{\theta 4}}^2}\, P_{t4} = P_{t1} - \frac{\rho_{t1}\Delta H_{id}(1-\eta_s)}{4} \quad (10)$$

It is assumed that theoretically the total enthalpy at the rotor inlet (H_4) is equal to the total enthalpy at the inlet volute (H_1). Since the velocity at the inlet volute (station 1) is small compared to that in the other stations, it can be assumed that the total pressure in that station (P_{t1}) is equal to the static pressure (P_1). The equation of state that relates the density (r_4), static enthalpy (h_4), and static pressure (P_4) at the inlet of the blade rotor is needed. For this purpose, *Computer-Aided Thermodynamics Tables 3* (CATT3) are used [20,21]. The iteration is carried out until the r_4, and h_4 reach their convergent values.

Once the inlet rotor radius (r_4) is known, the inlet and outlet blade thickness and hub radius can be obtained from these following equation [17]:

$$t_{b4} = 0.04r_4 \; t_{b5} = 0.02r_4 \; r_{h5} = 0.185r_4 \quad (11)$$

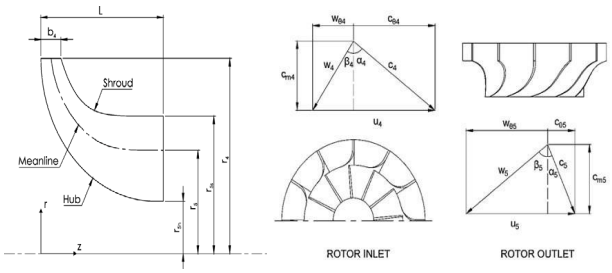

(a) **(b)**

Figure 3 (a) Meridional Section sketch of a rotor (b) Velocity Triangle detail on rotor passage

The outlet shroud radius (r_{s5}) is calculated from and the rotor axial length (ΔZ_R) is calculated from

$$\frac{r_{s5}}{r_4} \leq 0.78 \quad (12)$$

$$\Delta Z_R = 1.5(r_{s5} - r_{h5}) \quad (13)$$

The number of blades and the inlet blade angle can be calculated from

$$N_R = \frac{\pi(110 - \alpha_4) \, tan \, tan \, \alpha_4}{30} \quad (14)$$

$$\beta_4 = \left(\frac{C_{\theta 4} - U_4}{C_{m4}}\right) \quad (15)$$

Rotor outlet radius (r_5) and outlet passage width (b_5) are obtained from following equations [17]

$$r_5 = \frac{r_{s5} + r_{h5}}{2} \quad (16)$$

$$b_5 = r_{s5} - r_{h5} \quad (17)$$

The pitch distance between each blade at rotor outlet s_5 is obtained from following equation:

$$s_5 = \frac{2\pi r_5}{N_R} \quad (18)$$

If the Mach number at the rotor outlet is less than 1, then the throat width, o_5, is calculated from

$$o_5 = \frac{s_5 C_{m5}}{W_5} \quad (19)$$

$$C_{m5} = \frac{\dot{m}}{2\pi r_5 \rho_5 C_{m5}} \quad (20)$$

The density of fluid r_5 is calculated iteratively using *Computer-Aided Thermodynamics Tables 3* (CATT3) [22, 23] and the enthalpy equation

$$h_5 = H_5 - \frac{1}{2}C_{m5} \quad (21)$$

Iterative calculation is done until C_{m5^5} reaches its convergent value. Then the relative velocity at the rotor outlet, W_5, is calculated from

$$W_5 = \sqrt{{C_{m5}}^2 + r_5\omega^2} \tag{22}$$

To get the best efficiency, $C_{\theta 5}$ is set equal to zero, hence the outlet blade angle can be calculated from

$$\beta_5 = \left(\frac{C_{m5}}{W_5}\right) \tag{23}$$

Some dimensions should be checked so that the dimensions are within practical limits. The rotor axial length should be in the range [17]. It is also important to keep the $\frac{o_5}{s_5} < 1$ to avoid choking.

$$\Delta Z_R \geq 1.5 b_4 \tag{24}$$

The ratios of rotor outlet meridional velocity to rotor inlet absolute velocity and ratio of outlet to inlet meridional velocity are given by [22,23]:

$$0.2 \leq \frac{C_{m5}}{U_4} \leq 0.4\ 1 \leq \frac{C_{m5}}{C_{m4}} \leq 1.5 \tag{25}$$

The rotor stage reaction should be in the range [22]

$$0.45 \leq R \leq 0.65 \tag{26}$$

$$R = \frac{h_4 - h_5}{H_1 - H_5} \tag{27}$$

The shroud outline is drawn using the following equation:

$$r = r_{s5} + (r_4 - r_{s5})\xi^n; 2 \leq n \leq 9 \tag{28}$$

$$\xi = \frac{(z - z_5)}{\Delta Z_R - b_4} \tag{29}$$

Where *z* is a step size value between 0 and $\Delta z_R - b_4$. The step size is determined arbitrarily. The hub outline is made by Making a quarter circle with radius $r_4 - r_{5h}$ and its center located on a point that is parallel with the inlet station and adding a straight-line segment to the exit or creating a quarter circle with radius $\Delta Z_R$and its center located on a point that is parallel to the outlet station and adding a straight-line segment to the inlet. After the *r* and *z* values were determined, they were imported to Autodesk Inventor (AI) to generate the shroud and hub outline coordinates for the further design process and drawing creating 2D blade geometry. The illustration of this process both by two available methods were shown by Figure 4.

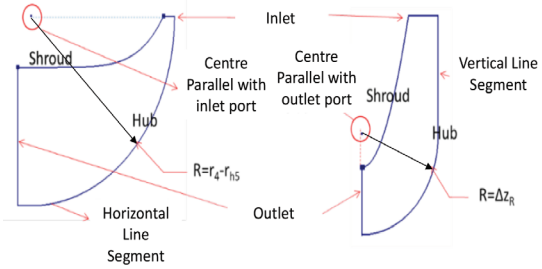

Figure 4 Detail section of rotor blade

2D blade geometry was transformed into 3D by dividing streamlines into equal parts. The numbers of streamlines and quasi normal lines are taken arbitrarily. The intersection between the quasi-normal lines with the shroud, hub and streamlines create the coordinate points of the blade. For each point, the twist angle or polar angle ($\theta_{j,i}$), the blade angle ($\beta_{j,i}$) and the tangential angle of the lines to the axial direction ($\phi_{j,i}$) are then calculated. Referring to Figure 5, *i* = *1,2,3,…….n* and *j* = *h, a, b, c, s*.

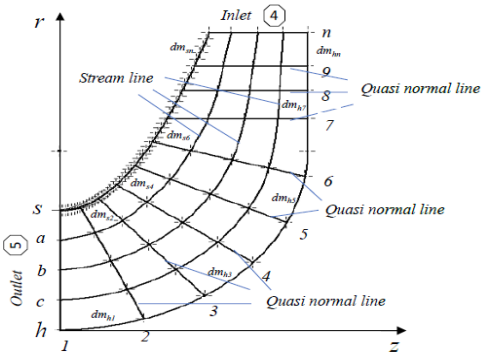

Figure 5 Shroud, streamlines, and quasi normal lines

Streamline was constructed graphically but can also be made by GAMBIT [21]. The quasi-normal line was constructed by selecting several *z* values in the shroud, after which the *r* ordinates were taken from the *Autodesk Inventor* (*AI*) drawing. The polar angles for each point along the shroud line ($\theta_{s,i}$) were calculated from [17]:

$$\begin{aligned}\theta_{s,i}(m_{s,i}) &= Am_{s,i} + B{m_{s,i}}^3 + C{m_{s,i}}^4\, m_{s,i+1} \\ &= m_{s,i} + dm_{s,i}m_{s,1}\end{aligned} \tag{30}$$

$$dm_{s,i} = \sqrt{\left(dz_{s,i}\right)^2 + \left(dr_{s,i}\right)^2} \tag{31}$$

$$\begin{aligned}A &= \frac{cot\ cot\ \beta_{5s}}{r_{5s}} \\ B &= \frac{1}{{m_4}^2}\left[\frac{cot\ cot\ \beta_4}{r_4} - \frac{cot\ cot\ \beta_5}{r_{5s}}\right] \\ C &= -\frac{B}{2m_4}\end{aligned} \tag{32}$$

$$r_{5s}\ tan\ tan\ \beta_{5s}\ = r_5\ tan\ tan\ \beta_5\ = r_{5h}\ tan\ tan\ \beta_{5h} \tag{33}$$

$$\theta_{h,i}(m_{s,i}) = Dm_{h,i} + E{m_{h,i}}^3 + F{m_{h,i}}^4 \tag{34}$$

Where *i* and $m_{h,i}$are calculated similarly as $m_{s,i}$

$$\begin{aligned}D &= \frac{cot\ cot\ \beta_{5h}}{r_{5h}} \\ E &= \frac{3\theta_4}{{m_4}^2} - \frac{1}{m_4}\left[\frac{2\ cot\ cot\ \beta_{5h}}{r_{5h}} + \frac{cot\ cot\ \beta_4}{\beta_4}\right] \\ F &= \frac{1}{{m_4}^2}\left[\frac{cot\ cot\ \beta_{5h}}{r_{5h}} + \frac{cot\ cot\ \beta_4}{\beta_4}\right] - \frac{2\theta_4}{{m_4}^3}\end{aligned} \tag{35}$$

The blade angle ($\beta_{j,i}$) and the tangential angle ($\phi_{j,i}$) of each point along the shroud, hub and every intersection point of the streamlines and the quasi-normal lines can be determined from

$$cot\ cot\ \beta_{j,i}\ = r_{j,i}\frac{d\theta_{j,i}}{dm_{,j,i}}\ sin\ sin\ \phi_{j,i}\ = \frac{dr_{j,i}}{dm_{,j,i}} \tag{36}$$

Referring to Figure 5, the coordinates of the points in the shroud and hub lines can be calculated from the following equations:

$$\tau_{j,i} = \frac{\phi_{j+1,i} + \phi_{j-1,i}}{2} \tag{37}$$

$$x_{s,i} = r_{s,i}\ sin\ sin\ \theta_{s,i}\ \ y_{s,i} = r_{s,i}\ cos\ cos\ \theta_{s,i} \tag{38}$$

$$x_{h,i} = r_{h,i}\ sin\ sin\ \theta_{h,i}\ \ y_{h,i} = r_{h,i}\ cos\ cos\ \theta_{h,i} \tag{39}$$

The coordinates of the streamline and quasi normal line intersections can be obtained from

$$\begin{aligned} x_{h,i} &= x_{h,i} + (x_{s,i} - x_{h,i})\varphi_{j,i}\ y_{h,i} \\ &= y_{h,i} + (y_{s,i} - y_{h,i})\varphi_{j,i} \end{aligned} \tag{40}$$

$\varphi_{j,i}$ is the fraction length of the quasi normal line from the intersection point to the hub. $\varphi_{j,i} = 0$ and $\varphi_{j,i} = 0$ indicates the intersection point at the hub line shroud respectively. The ordinates *r* and *z* of the points are obtained from the AI drawing. Figure 6 shows the blade parameters and coordinates.

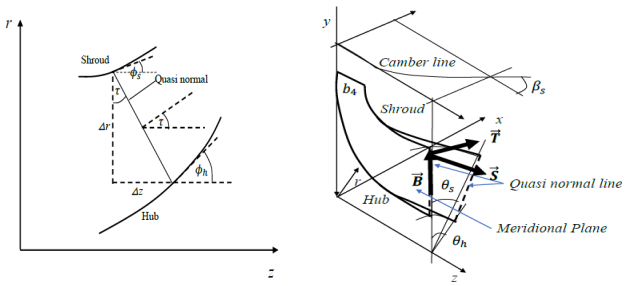

(a) (b)

Figure 6 (a) Sketch of quasi normal line position on 2D meridional component (b) 3D Rotor meridional geometry component

The points discussed above are then transformed into three-dimensional coordinates by using vector operation. Three kinds of vectors are defined, i.e. [17]: the vector tangential to the blade profile along the meridional direction ($\vec{S}_{j,i}$), the vector along a quasi-normal line ($\vec{B}_{j,i}$), and the vector that is perpendicular to the blade profile ($\vec{T}_{j,i}$) and defined as equation below:

$$\begin{aligned} \vec{S}_{j,i} &= S_{x,j,i}\hat{\imath} + S_{y,j,i}\hat{\jmath} + S_{z,j,i}\hat{k}\ \vec{B}_{j,i} \\ \vec{B}_{j,i} &= B_{x,j,i}\hat{\imath} + B_{y,j,i}\hat{\jmath} + B_{z,j,i}\hat{k}\ \vec{T}_{j,i} \\ \vec{T}_{j,i} &= S_{x,j,i} \times \vec{B}_{j,i} = T_{x,j,i}\hat{\imath} + T_{y,j,i}\hat{\jmath} + T_{z,j,i}\hat{k} \end{aligned} \tag{41}$$

The vectors are calculated for each intersection point in the shroud, hub and other intersections of the streamlines and the quasi-normal lines. The components of vector $\vec{S}_{j,i}$ can be calculated from equations below:

$$\begin{aligned} S_{x,j,i} &= sin\ \sin\theta_{j,i}\ sin\ \sin\phi_{j,i}\ sin\ \sin\beta_{j,i} + \\ &\quad cos\ \cos\theta_{j,i}\ cos\ \cos\beta_{j,i}\ \ S_{y,j,i} \\ &= coscos\ cos\ \theta_{j,i}\ \ sinsin\ sin\ \phi_{j,i}\ \ sinsin\ sin\ \beta_{j,i}\ \ -sin \\ &\quad sin\ sin\ \theta_{j,i}\ coscos\ cos\ \beta_{j,i}\ \ S_{z,j,i} \\ &= sin\ sin\ \phi_{j,i}\ \ sin\ sin\ \beta_{j,i} \end{aligned} \tag{42}$$

The component vector $\vec{B}_{j,i}$ for the points in the shroud and the hub are calculated from:

$$\begin{aligned} B_{x,s,i} = B_{x,h,i} &= \frac{x_{s,i} - x_{h,i}}{L}\ B_{y,s,i} \\ = B_{y,h,i} &= \frac{y_{s,i} - y_{h,i}}{L}\ B_{z,s,i} \\ = B_{z,h,i} &= \frac{z_{s,i} - z_{h,i}}{L} \end{aligned} \tag{43}$$

$$L = \sqrt{(x_{s,i} - x_{h,i})^2 + (y_{s,i} - y_{h,i})^2 + (z_{s,i} - z_{h,i})^2} \tag{44}$$

Then, the component vector $\vec{B}_{j,i}$ and $\vec{T}_{j,i}$ for the other intersection points are calculated from:

$$B_{x,j,i} = sin\ sin\ \theta_{j,i}\ \ B_{y,j,i} = cos\ cos\ \theta_{j,i}\ \ B_{z,j,i} = 0 \tag{45}$$

$$\begin{aligned} T_{x,j,i} &= S_{z,j,i}B_{y,j,i} - S_{y,j,i}B_{z,j,i}\ T_{y,j,i} \\ &= S_{x,j,i}B_{z,j,i} - S_{y,j,i}B_{z,j,i}\ T_{z,j,i} \\ &= S_{x,j,i}B_{x,j,i} - S_{x,j,i}B_{y,j,i} \end{aligned} \tag{46}$$

The coordinates of points on the blade $x_{j,i}, y_{j,i}, z_{j,i}$ are the middle points. Vector transformation above will form a cross section of the blade at quasi normal lines by connecting the points calculated by the Equations below with straight lines. Figure 7 shows the blade transformation from 2D to 3D geometry:

$$[x_{j,i}{}^{\pm}\ y_{j,i}{}^{\pm}\ z_{j,i}{}^{\pm}] = [x_{j,i}\ y_{j,i}\ z_{j,i}] \pm \frac{1}{2}t_b[T_{x,j,i}\ T_{y,j,i}\ T_{z,j,i}] \tag{47}$$

Where t_b is calculated from Equations (12) and changed linearly from t_{b4} to t_{b5}. The coordinates of the points that were calculated from Equations (48) were plotted in AI. The results are shown in Figure 7. Using the *Loft Surface-Patch Menu* in AI and taking the *Edge* option, the 3D blade image as shown in Figure 7(b, a) was created. With selection of *Stitch Surface to Solid* and *Revolve Menu* in AI, the image shown in Figure 7(b, b) was generated. Then using the *Circular Pattern Menu*, resulted in blade rotor as shown in Figure 7(b, c).

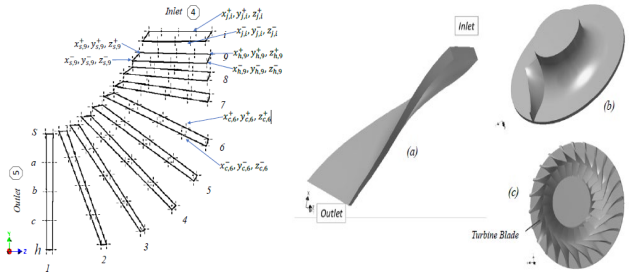

(a) **(b)**

Figure 7 (a) Transformation to 3D coordinates (b) 3D Rotor Figures Results

3.0 NOZZLE GEOMETRY

The nozzle geometry parameters are shown in Figures 8 (a) and 8(b). The input parameters of the calculation are b_4, α_4, r_4, $C_{\theta 4}$, ρ_4, N_R, and the mass flow rate is $\dot{m}$. The aforementioned parameters are obtained from Equations (6), (7), (9) to (12) and (20) above.

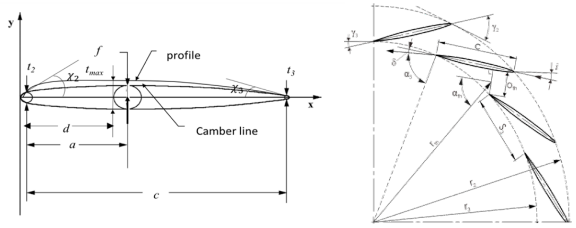

(a) (b)

Figure 8 (a) Nozzle blade profile (b) Parameters of guide nozzle

There is a gap between the blade rotor and the stator nozzle called the vaneless passage. The relation between r_3 and r_4 is expressed as [17]

$$\frac{r_3}{r_4} = 1 + \frac{K_1 b_4 \, sin\, sin\, \alpha_4}{r_4} \tag{48}$$

$K_1 = 2$ for optimum performance [24]. Then, the blade outlet angle α_3 can be calculated from

$$\alpha_3 = \frac{C_{m3}}{C_{\theta 3}} \tag{49}$$

$$C_{m3} = \frac{\dot{m}}{2\pi r_3 b_3 \rho_3} \tag{50}$$

$$C_{\theta 3} = \frac{C_{\theta 4} r_4}{r_3} \tag{51}$$

The outlet pitch of the nozzle (s_3) and number nozzle N_N and selection range of r_2 is calculated from [17].

$$s_3 = \frac{2\pi r_3}{N_N} \tag{52}$$

$$1.1 \le \frac{r_2}{r_3} \le 1.7 \tag{53}$$

To develop the nozzle blade profile, the camber line is used. The camber line is drawn using the following equation [17]:

$$y_c = \frac{x_c(c - x_c)}{\left[\frac{(c-2a)^2}{4b^2} + \frac{c-2a}{b} x_c - \frac{c^2 - 4ac}{4b}\right]} \tag{54}$$

Referring to Figure 8, *a* and *b* are designated for location of maximum camber, and *c* is the nozzle blade chord length. The *a*, *b*, and *c* are determined iteratively using the following equations:

$$0.25 \le \frac{a}{c} \le 0.75 \tag{55}$$

$$\frac{b}{c} = \frac{\left[\sqrt{1 + (4\, tan\, tan\, \eta)^2 \left(\frac{a}{c} - \left(\frac{a}{c}\right)^3 - \frac{3}{16}\right)}\right] - 1}{4\, tan\, tan\, \eta} \tag{56}$$

where the camber angle of nozzle (η) is calculated:

$$\begin{aligned} \eta &= X_2 + X_3\, tan\, tan\, X_2 \\ &= \frac{4b}{4a - c}\, tan\, tan\, X_3 \\ &= \frac{4b}{3c - 4a} \end{aligned} \tag{57}$$

blade angle at the inlet (α_2) and the fluid inlet angle (β_2) are determined iteratively from:

$$\frac{4 s_3 \, sin\, sin\, (\beta_2 - \alpha_3)}{c \, sin\, sin\, \beta_2 \left[1 + \frac{r_3 \, sin\, sin\, \alpha_3}{r_2 \, sin\, sin\, \alpha_2}\right]} \le 1 \tag{58}$$

$$\beta_2 = \gamma_2 - X_2 \tag{59}$$

$$r_2\, cos\, cos\, \gamma_2 = r_3\, cos\, cos\, \gamma_3 \tag{60}$$

where g is the nozzle setting angle and the following equation for the length of the nozzle chord (c) is also used:

$$c = \frac{r_2 - r_3}{sin\, sin\, \gamma_3} \tag{61}$$

Once the camber line has been constructed, the nozzle profile line coordinates can be drawn using the following equations:

$$x = x_c \pm 0.5t \, sin\, sin\, K \quad y = y_c \pm 0.5t \, sin\, sin\, K \tag{62}$$

$$t = t_{ref} + (t_{max} - t_{ref})\xi^e \tag{63}$$

$$t_{ref} = t_2 + [t_3 - t_2]\left(\frac{x_c}{d}\right) \tag{64}$$

$$\begin{aligned} \xi = \{ & \frac{x_c}{d} \; for\; x \\ & \le d \; \frac{(c-x)}{(c-d)} \; for \; for\; x \ge d \end{aligned} \tag{65}$$

$$e = \sqrt{\frac{0.4d}{c}} \left[0.95\left(1 - \frac{x_c}{c}\right)(1 - \xi) + 0.05\right] \tag{66}$$

$$K = \left(\frac{\partial y_c}{\partial x_c}\right) \tag{67}$$

To solve some of the equations above, there are several values proposed by Aungier [17], i.e.:

$$\frac{t_2}{c} = 0.03;\; \frac{t_3}{c} = 0.015;\; \frac{t_{max}}{c} = 0.06\,;\frac{d}{c} = 0.4 \tag{68}$$

The upper profile was drawn by plotting the x^-, and y^+ coordinates while the lower profile was drawn using the x^+, and y^- coordinates. The coordinates were then imported to AI and the nozzle was positioned manually by placing the tip of the nozzle's leading edge on the outer circle of the nozzle passage and the trailing edge on the innermost circle. Once the coordinates were well placed, the coordinates were connected using the *Spline Menu* and then *Extrude* with a value of b_4. The tips of the nozzle were drawn with the *Tangent Arc Menu*. The surrounding nozzles were constructed using the *Circular Pattern Menu*.

4.0 VOLUTE GEOMETRY

This study will use external type volute. The volute geometry is shown in Figures 9 (a) and 9(b) while the input parameters to calculate the volute parameters were: the density of the fluid at the volute inlet r_1, the fluid mass flow rate ($\dot{m}$), and the following equations:

$$C_2 = \frac{c_{m2}}{sin\, sin\, \alpha_2}\,;C_{\theta 2} = \frac{c_{m2}}{tan\, tan\, \alpha_2}\,;C_{m2} = \frac{r_3 c_{m3}}{r_2} \tag{69}$$

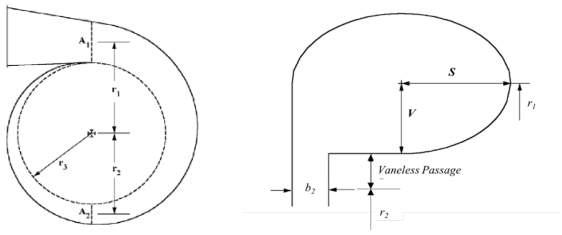

Figure 9 (a) Volute geometry (b) External elliptical volute

Then, the aspect ratio S/V is selected between 0.75 and 1.5. Inlet velocity A_1, C_1, S, r_1, and V are calculated iteratively from equations below:

$$\begin{aligned}\rho_1 C_1 A_1 &= \dot{m}\, r_1 C_1 = r_2 C_{\theta 1}\, A_1 \\ &= \left(\frac{3\pi}{4}+1\right) S \times V\, r_1 \\ &= r_2 + V + vaneless\ passage\end{aligned} \tag{70}$$

Once the volute parameters have been found, the cross-sectional area of the volute is calculated for various angles (ϕ) along 360°.

$$A_c = \frac{\phi}{2\pi} A_1\, V = \frac{A_c}{\left(\frac{3\pi}{4}+1\right) S}\, r_{max} = r_1 + V \tag{71}$$

Figure 10 shows the formation of the volute. The cross sections are developed every 30°, then the 3D surface is developed, covering the cross-sections. At the end of the process, an extended pipe is attached to the volute.

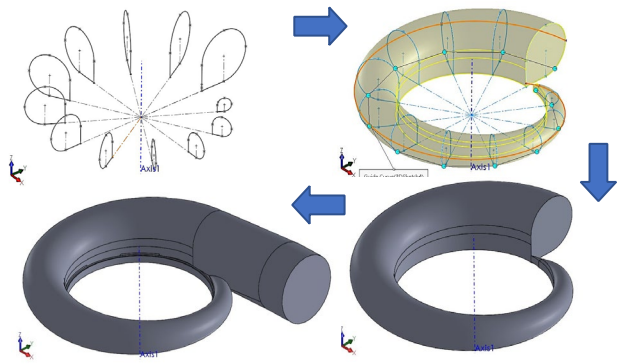

Figure 10 Formation of the volute

5.0 DESIGN RESULTS AND CONCLUSION

The radial inflow turbine from the design is shown in this section. A case study is shown in this paper with R134a as working fluid with following conditions: mass flow rate at 1-2 kg/s, inlet pressure at 1.5 to 5 bar, inlet temperature at 80 to 130 °C, and power output target between 20 to 25 kW. The detailed input parameters for designing the turbine are shown in Table 2 with the geometry results for rotor, nozzle and volute are shown in Table 3, Table 4, and Table 5 respectively. Figure 11 show the complete assembly of turbine generated from the design process

Table 2 Input Parameters for Rotor Geometry

Parameter	Symbol	Value Range
Fluid	-	R-134a
Inlet pressure	P_1	1.5-5 bar
Inlet temperature	T_1	80-130 ^{o}C
Mass flow rate	$\dot{m}$	1-2 kg/s
Power output target	P	20-25 kW
Rotational speed	ω	20,000 rpm

Table 3 Calculation Results of Turbine Rotor Parameters

Parameter	Symbol	Value	Unit
Specific speed	n_s	0.53	-
Inlet Mach number	M_4	0.18	-
Inlet rotor radius	r_4	0.059	m
Inlet blade thickness	*tb4*	0.002	m
Inlet passage width	b_4	0.013	m
Outlet blade thickness	*tb5*	0.001	m
Outlet hub radius	*r5h*	0.017	m
Outlet shroud radius	*r5s*	0.041	m
Rotor axial length	Δz_R	0.035	m
Rotor outlet radius	r_5	0.029	m
Outlet passage width	b_5	0.023	m
Outlet mean blade pitch	s_5	0.014	m
Number of blades	*N*	13	
Output rotor power	*P*	21.92	kW

Table 4 Input Parameters and Calculation Results for Nozzle Geometry

Input Parameters			
Parameter	**Symbol**	**Value**	**Unit**
Ratio of a/c	*a/c*	0.3	-
Inlet passage width	b_4	0.012	m
Inlet absolute flow angle	α_4	1.29	radian
Inlet rotor radius	r_4	0.058	m
Mass flow rate	$\dot{m}$	1.6	kg/s
Calculation Results			
Location of maximum camber line height	*a*	14.58	mm
Maximum height of camber line	*b*	28.01	mm
Camber line chord length	*c*	48.63	mm
Nozzle inlet tangential angle	χ_2	49.04	degrees
Nozzle outlet tangential angle	χ_3	7.29	degrees
Camber line angle	ϑ	56.34	degrees
Nozzle outlet radius	r_3	83.55	mm
Nozzle inlet radius	r_2	125	mm
Nozzle inlet angle	β_2	21	degrees

Table 5 Input Parameters and Calculation Results for Volute Geometry

Input Parameters			
Parameter	**Symbol**	**Value**	**Unit**
Mass flow rate	$\dot{m}$	1.6	kg/s
Nozzle inlet radius	r_2	0.125	m
Aspect Ratio	S/V	1.1	-
Calculation Results			
Parameter	**Symbol**	**Value**	**Unit**
Volute inlet passage area	A_1	0.003	m^2
Center point radius	r_1	0.154	m
Volute outlet radius	r_2	0.125	m
Volute maximum vertical length	S	0.032	m
Volute maximum horizontal length	V	0.029	m
Volute maximum radius	$rmax$	0.154	m

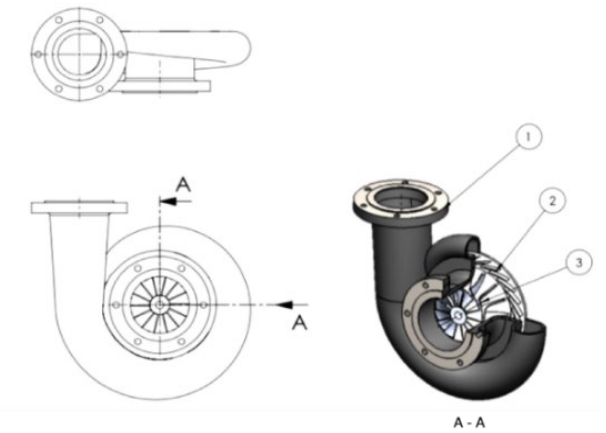

Figure 11 Radial Turbine geometry results: (1) Volute (2) Nozzle (3) Rotor

6.0 CFD SIMULATIONS

A 3D steady state flow simulation was performed in order to verify the design results. The 3D geometry design result of the turbine was exported to ANSYS Mesh to generate the computational grid. The result of computational grid generated were shown on Figure 12.

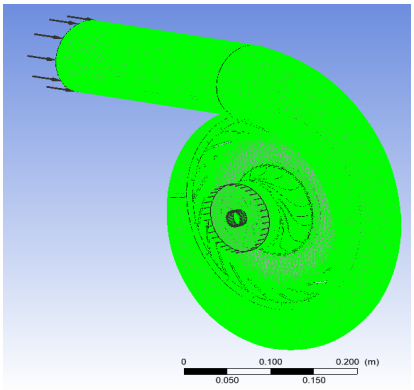

Figure 12 Turbine mesh and setup

ANSYS CFX was selected to perform the simulations. A turbulence model of $\kappa - \varepsilon$ was used for the turbulence model. For boundary conditions, the simulation used a total pressure inlet and static pressure outlet. The specific boundary was set into two conditions to improve the validation of this analysis. Condition A with rotor rated speed of 20,000 rpm, pressure inlet at volute inlet at 3.85 bar, an inlet temperature of 100°C, and pressure outlet at rotor outlet at 1.81 bar. Then, condition B was set with mass flow at Volute inlet while keeping the other condition the same as condition A. In this analysis, one dynamic interface was located between nozzle and rotor, defined as Mixing Plane model.

Figure 13 and 14 shows streamline distribution of radial turbine and streamline distribution at midspan of blade. From the figure, it can be seen that the flow to the nozzle is relatively smooth with relatively uniform distribution. The nozzle shows significant velocity changes located near the end of the nozzle blade, peaking at the nozzle exit. Slight reverse flow occurred in rotor entrance around pressure area and will only cause slight flow loss.

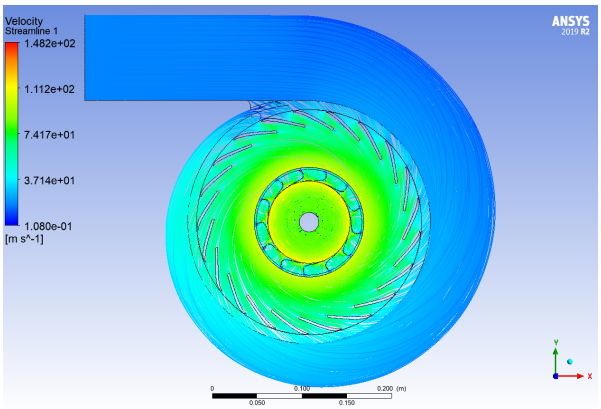

Figure 13 Radial turbine streamline

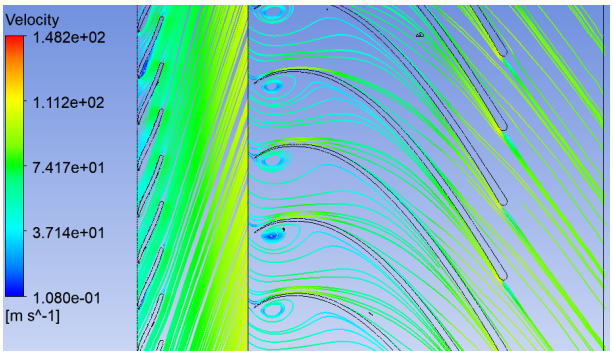

Figure 14 Blade to blade streamline at mean line (50% blade span)

Table 6 showing the comparison of design results and CFD results. The result shows that the design has good efficiency and similar condition results compared to theoretical design, thus validating the method used in this paper.

Table 6 Comparison of geometry design results

Parameter	Design Results	CFD Results A	CFD Results B
Rotation Speed / rpm	20,000	20,000	20,000
Fluid	R134a	R134a	R134a
Output Power / kW	21.92	20.22	35.07
Mass flow rate / kg/s	1.6	1.6	2,15
Isentropic Efficiency / %	86.94	92.56	86.36
Inlet Pressure (bar)	3.85	3.2	3.82
Static Outlet Pressure (bar)	1.81	1.81	1.80

Although the calculation methods discussed above provide a simple way to determine the radial inflow turbine geometry, further study is required to see the sensitivity of the assumed parameters. The coordinates of the turbine geometry can be easily imported into a 3D printing or additive machine for turbine production. To prove the validity of the method, turbine production and assembly engineering has to be done before a real test in an ORC system can be conducted to verify the performance of the turbine in the future.

Acknowledgement

The authors would like to thank Institut Teknologi Bandung for providing financial support for this research.

References

[1] Barai. M.K, Saha. B.B. 2005. En*ergy Security and Sustainability in Japan.* 2. 49–56. DOI: https://doi.org/10.5109/1500427

[2] Faisal. M, Baran. B, Khanam, M. Faisal Hasan, M, Miyazaki. T, Baran Saha, B, Koyama S. 2018. Key Factors of Solar Energy Progress in Bangladesh Until 2017. Ev*ergreen - Joint Journal of Novel Carbon Resource Sciences & Green Asia Strategy.* 05: 78–85. DOI: https://doi.org/10.5109/1936220

[3] Sharma. M, Dev. R. 2018. Review and Preliminary Analysis of Organic Rankine Cycle based on Turbine Inlet Temperature. *Evergreen - Joint Journal of Novel Carbon Resource Sciences & Green Asia Strategy*. 5: 22–33. DOI: https://doi.org/10.5109/1957497

[4] Siregar. U.J, Arif. M.F, Suryana. J, Indartono.Y.S. 2018. IOP Conference Series: Earth and Environmental Science Potential of biomass as source for electricity at Pulau Panggang Village, North Kepulauan Seribu Subdistrict. *IOP Conference Series: Earth and Environmental Science.* 196: 12027. DOI: http://dx.doi.org/10.1088/1755-1315/196/1/012027

[5] Qiu. G. 2012. Selection Of Working Fluids for Micro-CHP Systems With ORC. *Renewable Energy*, 48: 565–570. DOI: https://doi.org/10.1016/j.renene.2012.06.006

[6] Alshammari. F, Pesyridis. A, Karvountzis-Kontakiotis. A, Franchetti. B, Pesmazoglou. Y. 2018. Experimental Study of a Small-Scale Organic Rankine Cycle Waste Heat Recovery System for a Heavy-Duty Diesel Engine with Focus on The Radial Inflow Turbine Expander Performance. *Applied Energy.* 215: 543–555. DOI: https://doi.org/10.1016/j.apenergy.2018.01.049

[7] Song.J, Gu.C, Ren.X. 2016. Influence of the Radial-Inflow Turbine Efficiency Prediction on The Design and Analysis of The Organic Rankine Cycle (ORC) System. *Energy Conversion and Management*. 123: 308–316. DOI: https://doi.org/10.1016/j.enconman.2016.06.037

[8] Fiaschi. D, Manfrida. G, Maraschiello. F. 2015. Design And Performance Prediction of Radial ORC Turboexpanders. *Applied Energy*. 138: 517–532. DOI: https://doi.org/10.1016/j.apenergy.2014.10.052

[9] Kang. S.H. 2012. Design And Experimental Study of ORC (Organic Rankine Cycle) And Radial Turbine Using R245fa *Working Fluid. Energy*. 41: 514–524. DOI: https://doi.org/10.1016/j.energy.2012.02.035

[10] Al Jubori. A.M, Al-Dadah R.K, Mahmoud.S, Daabo. A. 2017. Modelling And Parametric Analysis of Small-Scale Axial and Radial-Outflow Turbines for Organic Rankine Cycle Applications. *Applied Energy*. 190: 981–996. DOI: https://doi.org/10.1016/j.apenergy.2016.12.169

[11] Costall. A.W, Hernandez. A.G, Newton. P.J. 2015. Design Methodology for Radial Turbo Expanders in Mobile Organic Rankine Cycle Applications. *Applied Energy*. 157: 729–743. DOI: https://doi.org/10.1016/j.apenergy.2015.02.072

[12] Arifin. M, Pasek. A.D. 2015. Design Of Radial Turbo-Expanders for Small Organic Rankine Cycle Systems. *IOP Conference Series: Materials Science and Engineering*. 88: 012037. DOI: https://doi.org/10.1088/1757-899X/88/1/012037

[13] Aungier. R.H. 2006.Turbine Aerodynamics: Axial-Flow and Radial-Inflow Turbine Design and Analysis; ASME Press: New York. DOI: https://doi.org/10.1115/1.802418

[14] Zahed. A.H. 2015, Bayomi, N.N. Radial Turbine Design Process; ISESCO *Journal of Science and. Technology,* 11(19): 9-22.

[15] Ventura. C.A.M, Jacobs P.A, Rowlands. A.S, Petrie-Repar, P. Sauret. E. 2012. Preliminary Design and Performance Estimation of Radial Inflow Turbines: An Automated Approach. J*ournal of Fluids Engineering. ASME*. 134. DOI: https://doi.org/10.1115/1.4006174

[16] Wu. H.Y, Pan. K.L. 2018. Optimum Design and Simulation of a Radial-Inflow Turbine for Geothermal Power Generation. *Applied Thermal Engineering.* 130: 1299–1309. DOI: https://doi.org/10.1016/j.applthermaleng.2017.11.103

[17] Li. Y, Ren, X.D. Investigation of The Organic Rankine Cycle (ORC) System and The Radial-Inflow Turbine Design. 2016*. Applied Thermal Engineering.* 96: 547–554. DOI: https://doi.org/10.1016/j.applthermaleng.2015.12.009

[18] Rahbar, K.; Mahmoud, S.; Al-dadah, R.K.; Moazami, N. 2015. Parametric Analysis and Optimization of a Small-Scale Radial Turbine for Organic Rankine Cycle. *Energy***.** 83: 696–711. DOI: https://doi.org/10.1016/j.energy.2015.02.079

[19] Shao, S, Deng. Q, Shi. H, Feng. Z, Cheng. K, Peng. Z. 2013. Numerical Investigation on Flow Characteristics of Low-Pressure Exhaust Hood Under Off-Design Conditions for Steam Turbines. Proceedings of the ASME Turbo Expo 2013: Turbine Technical Conference and Exposition. Volume 5B: Oil and Gas Applications; Steam Turbines. San Antonio. l. 5 B. V05BT25A031. DOI: https://doi.org/10.1115/GT2013-95257

[20] Richard E Sonntag, C Borgnakke, Gordon J Van Wylen, IntelliPro. 1994. Computer Aided Thermodynamic Tables 3. Wiley, New York.

[21] R.P. Putri. 2018. Study on Designing 250 Kw Radial Inflow Turbine in Organic Rankine Cycle with Propane as Working Fluid. Master Program Thesis, Institut Teknologi Bandung, Bandung.

[22] Balje. O.E. 1981. Turbomachines. A Guide to Design, Selection and Theory. John Wiley & Sons Inc. United States. DOI: https://doi.org/10.1115/1.3241788

[23] Wood. H.J. 1963. Current Technology of Radial-Inflow Turbines for Compressible Fluids. *Journal of Engineering for Gas Turbines and Power*. 85: 72–83. DOI: https://doi.org/10.1115/1.3675226

[24] H.F.Basri. 2018. Perancangan Dan Analisis CFD Turbin Radial Inflow Dengan Daya 50 KW pada Siklus Rankine Organik Sederhana Dengan Fluida Kerja R1233zd(E), Bachelor's Thesis. Institut Teknologi Bandung

[25] Y. Chen, Y. Liu, L. Zhang, and X. Yang, 2021. Three-Dimensional Performance Analysis of a Radial–Inflow Turbine for Ocean Thermal Energy Conversion System. *Journal of Marine Science and Engineering*, . 9(3): 287. DOI : https://doi.org/10.3390/jmse9030287